Contents lists available at ScienceDirect

Sensors and Actuators A: Physical

journal homepage: www.elsevier.com/locate/sna

Micromachined chip-scale plasma light source

P. Carazzetti, Ph. Renaud, H. Shea*

Ecole Polytechnique Fédérale de Lausanne (EPFL), 1015 Lausanne, Switzerland

ARTICLE INFO

Article history:
Received 1 April 2008
Received in revised form 22 May 2008
Accepted 28 May 2008
Available online 6 June 2008

Keywords:
Plasma
Interdigitated electrodes
Anodic bonding
Hermetic sealing
Light source
Impedance matching
Spectroscopy
Micromachining
Aluminum electrodes

ABSTRACT

We report on the microfabrication and testing of a chip-scale plasma light source. The device consists of a stack of three anodically bonded Pyrex wafers, which hermetically enclose a gas-filled cavity containing interdigitated Aluminum electrodes. When the electrodes are powered through an impedance matching circuit, these devices have been used to generate stable millimeter-size RF plasma discharges operating continuously for over 24 h in He or Ar at pressures ranging from 10 to 500 mbar at RF powers of 300–1500 mW.

1. Introduction

Plasma discharges can be very efficient and stable light sources, for instance widely used as pixels in plasma TVs (<1 W/pixel), as Rubidium lamps in commercial compact Rb atomic frequency standards (few W), or even proposed as bright sources for EUV lithography (>10 W). Plasma discharge light sources can offer long lifetimes, important for applications such as atomic clocks. Although lasers offer higher optical efficiency, commercial Rb atomic clocks rely on Rb discharge lamps because of their very slow frequency drift (aging) and long lifetime.

Research to date on micromachined plasma source has been on *unsealed* electrode arrays, typically atmospheric plasmas for medical or chemical applications [1–3], gas chromatography [4] or spectroscopy [5,6]. We have developed a *sealed* chip-scale plasma light source that is low power (as required for portable applications), versatile and compact, with efficient operation at 10–500 mbar in different gases (Ar, He and N_2) [7]. For chemical or biological applications, the small size of a micromachined plasma source allows integration or co-fabrication with microfluidic devices. For chip-scale atomic clocks the benefit of a compact stable light source is obvious.

Micromachining technologies allow the fabrication on the wafer scale of small gaps (1–500 μm) between electrodes, which enables generating the high electric fields (of order 2×10^7 V/m) required to ignite gas discharges using reasonable DC or RF voltages (100–400 V). The Paschen curve [8] provides a good starting point for estimating the DC voltage required to ignite a plasma. Significant deviations from the Paschen curve are reported for gaps smaller than 5 μm due to field emission [9–14]. At larger gaps deviations are also reported, in particular for RF operation because of the additional length scales brought into play for RF operation [17]. A study of DC breakdown voltage for different electrode configurations to measure the Paschen curve at reduced pressures for gaps from 10 to 500 μm is reported in [15].

RF operation (near 20 MHz) was chosen for our plasma light source in order to extend device lifetime by minimizing the erosion of the cathode that occurs with DC plasmas [16] from ion bombardment. For RF operation ions are only accelerated to the cathode during one half-period of the RF cycle and thus generally do not reach the cathode. Additionally RF operation allows the use of passivated electrodes. It has been reported that RF operation also reduces the power needed for ignition [17]. We minimized the RF power required for ignition and stable operation by patterning sharp corners in the electrodes and by using an on-PCB circuit to match the capacitive impedance ($Z > 1$ kΩ) of the chips to the 50 Ω RF source, while also providing more than a factor of 50 of voltage amplification.

* Corresponding author.
E-mail address: herbert.shea@epfl.ch (H. Shea).

0924-4247/$ – see front matter © 2008 Elsevier B.V. All rights reserved.
doi:10.1016/j.sna.2008.05.028

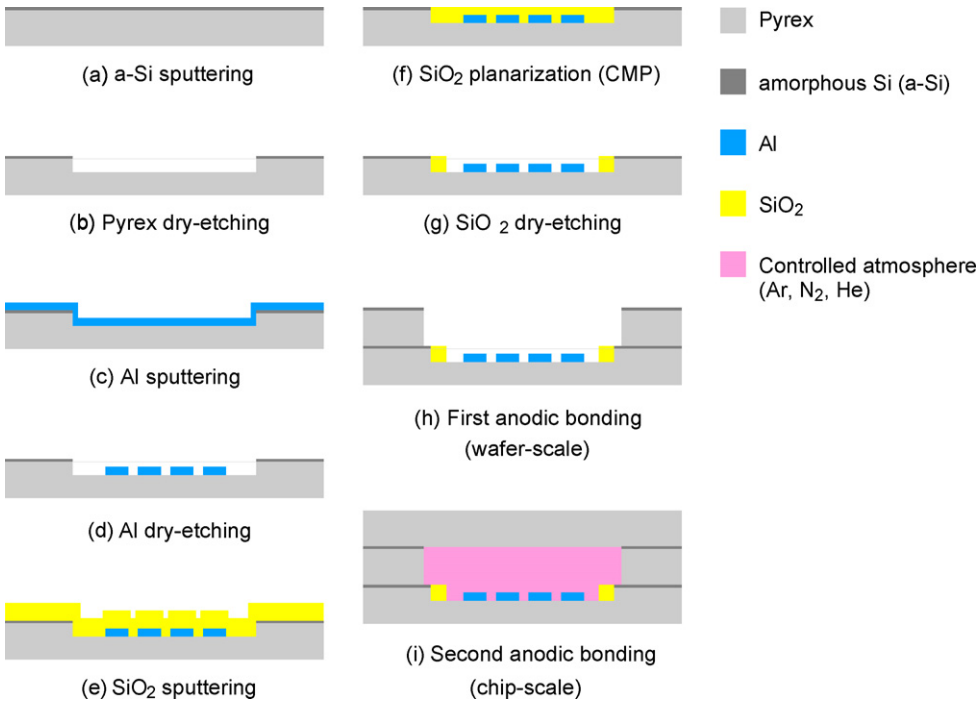

Fig. 1. Schematic process flow. All substrates are 100-mm Pyrex wafers with a thickness of 500 μm.

The paper is organized as follows: the device microfabrication is presented in Section 2. The impedance matching is discussed in Section 3. Data on plasma generation, optical power and lifetime are presented in Section 4.

2. Fabrication

The key features of the microfabrication process are: the use of powder blasting on Pyrex as a versatile technology to create through-wafer holes of any geometry on the same substrate (unlike ultrasonic drilling), and the use of Pyrex-to-Pyrex anodic bonding to create hermetic cavities. A cross-section of the process flow is shown in Fig. 1.

As a first step, 2 μm of amorphous silicon (a-Si) are sputtered on a 100-mm Pyrex wafer (Wafer#1) and patterned by dry-etching. This film acts as a mask for the subsequent dry-etch of 2 μm-deep cavities in Pyrex. To enable anodic bonding, the a-Si is not removed [18]. Next, 3 μm of Aluminum are sputter deposited and interdigitated electrodes are dry-etched in the cavities using an inductively coupled plasma (ICP) process based on Cl_2/BCl_3 chemistry. Fig. 2a shows typical anisotropic patterns with very sharp corners enabled by the ICP process. Wafer#1 is then coated with 4 μm of sputtered SiO_2 and chemical–mechanical polishing (CMP) is performed with a stop on the remaining a-Si film. SiO_2 is then etched in CF_4 plasma, which is highly selective towards Al, in order to open via-holes for electrical contacts and to locally remove residual SiO_2 from the electrode area (Fig. 2b). It is also possible to leave the SiO_2 on the electrodes should passivated electrodes be preferred. A first anodic bonding is performed at 350 °C and 1.2 kV between Wafer#1 and a second Pyrex substrate (Wafer#2). The latter has through-wafer holes created by powder blasting (Fig. 2c) [19]. In this process, the Pyrex surface, which is protected with a photolithographically defined polymer mask, is eroded by a jet of alumina particles with a diameter of 30 μm. The etch-rate of Pyrex achieved in static mode is 50 μm/s. Furthermore, unlike wet-etching, powder blasting avoids mask undercutting thus enabling the fabrication of anisotropic holes with wall angles of about 15–18°. According to the manufacturer [20], a processing time of about 1 h and 45 min is required for blasting an array of through-wafer holes in a 500 μm-thick Pyrex substrate with diameter of 100-mm.

The bonded stack (Fig. 2d) is then diced into 10 mm × 10 mm chips. Using the previously mentioned conditions, a second anodic bonding is performed under a controlled gas pressure to a third Pyrex chip acting as a lid in order to hermetically seal the cell enclosing the electrodes (Fig. 2f). Again, Pyrex-to-Pyrex anodic bonding is made possible by the a-Si film (100 nm) deposited on Wafer#2 before powder blasting. The low temperature used for the anodic bonding protects the Al electrodes while enabling an excellent adhesion between bonded wafers.

This final bonding step to seal the cell can be performed on the wafer-scale, or the final bonding can be performed chip by chip, resulting in devices in Fig. 2e and then Fig. 2f, depending on how the cell is to be filled. For instance, for filling with Rubidium, a chip-scale approach might be preferred, while for filling simply with a given gas pressure, a wafer-scale solution could be chosen.

3. Impedance matching

The impedance matching network shown in Fig. 3 has been implemented on a PCB (printed circuit board) and serves two purposes: (1) to allow maximum power transfer from the $Z_s = 50\,\Omega$ source (a variable gain 10 W RF amplifier 1–500 MHz, model BBM1C3KAJ, Empower RF Systems, Inc.) to the load, Z_{chip}, corresponding to the >1 kΩ capacitive impedance of the chip, and (2) to amplify the voltage from the amplifier in order to reach the 200–300 V needed to ignite the plasma discharge (500 mW into 50 Ω corresponds to 5 V peak voltage).

The main challenge with this circuit is designing and tuning it such that both the maximum in the voltage amplification and the matching to 50 Ω occur at the same frequency. The discrete components (inductors and capacitors) must have sufficiently high quality factors at those frequencies. Fig. 4 is a simulation obtained using the PSpice tool [21] of the circuit in Fig. 3, including a number of parasitics to account for stray capacitances, wire-bonds inductance

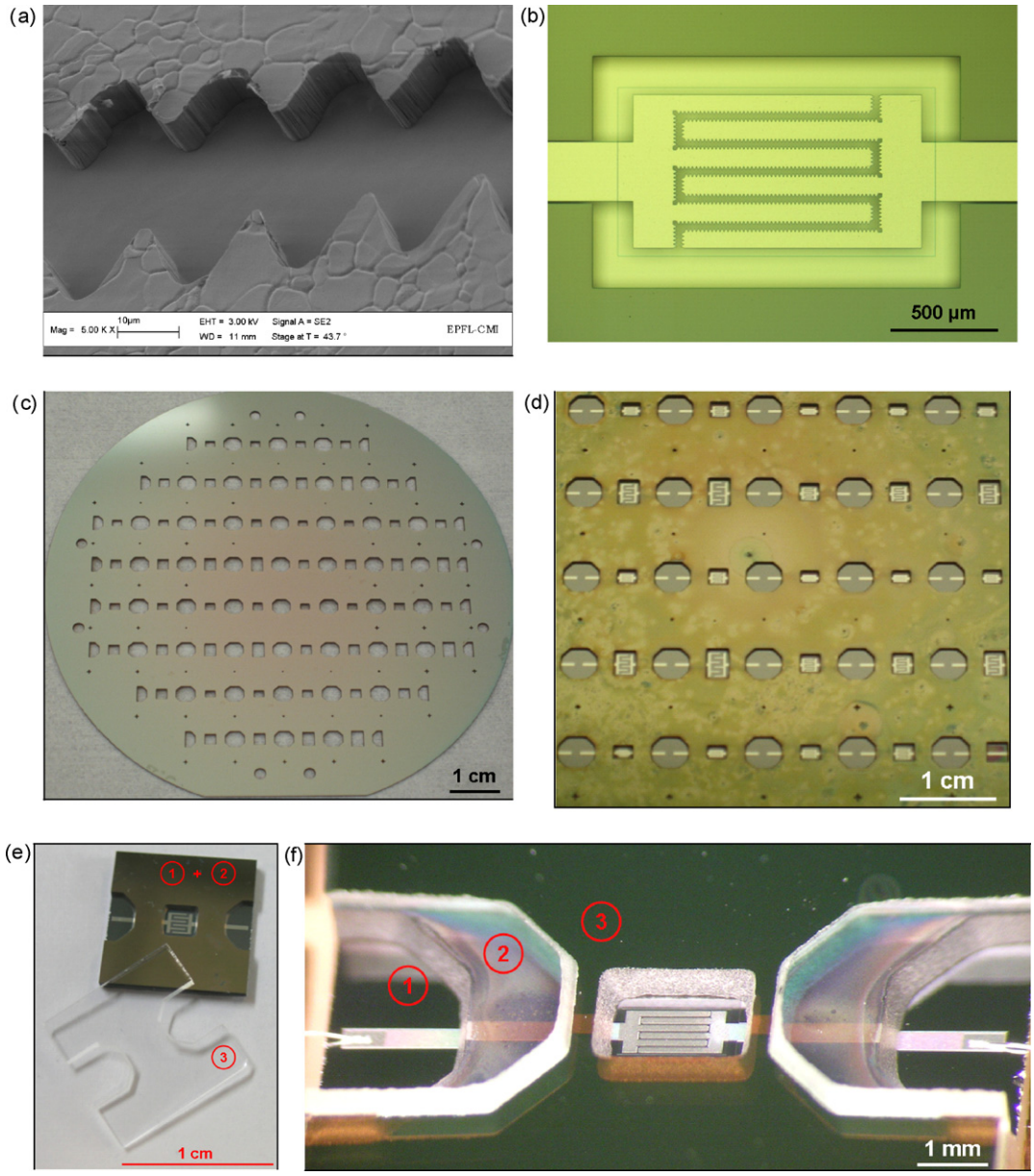

Fig. 2. Details of the fabrication process: (a) SEM micrograph of dry-etched Al electrodes, (b) Pyrex cavity with interdigitated electrodes after CMP and SiO_2 etching (Wafer#1), (c) powder blasted Pyrex wafer coated with 100 nm of amorphous Si (Wafer#2), (d) Wafer#1 and Wafer#2 after the first anodic bonding, (e) diced chips ready for final bonding, the wafer number is circled, and (f) final sealed triple-stack chip, the wire-bonds to the PCB are visible.

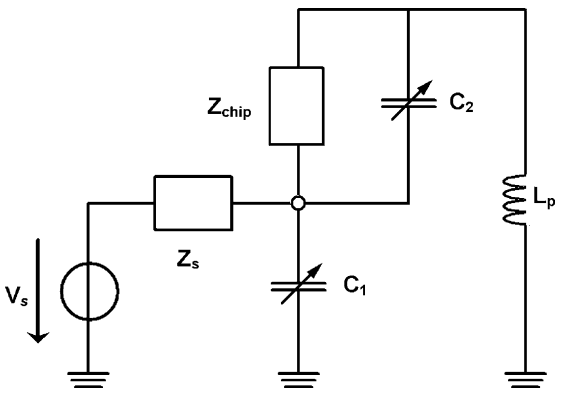

Fig. 3. Equivalent circuit used for impedance matching.

and the series resistances of the metal traces. Real and imaginary components of the circuit impedance, as well as the voltage amplification on the chip are plotted as a function of frequency. In this simulation the voltage peak occurs at 21.2 MHz, which is the frequency where $\mathrm{Re}(Z) = 50\,\Omega$ for which the power transfer will be maximized.

The impedance matching circuit of Fig. 3 is implemented using two trimmer capacitors (C_1: 5–110 pF and C_2: 1.2–6 pF) and a fixed inductor ($L_p = 10\,\mu H$). After a chip is mounted on the impedance-matching PCB (see Fig. 5), the circuit's impedance is measured with a network analyzer (HP 8753D) and displayed in Smith chart form, while the trimmer capacitors are tuned until 50 Ω purely resistive impedance is obtained. This determines the operating frequency that will be later programmed on the signal generator (HP 8642A) to ignite the RF discharge. Fig. 6 shows the Smith chart corresponding to the measured impedance of the circuit

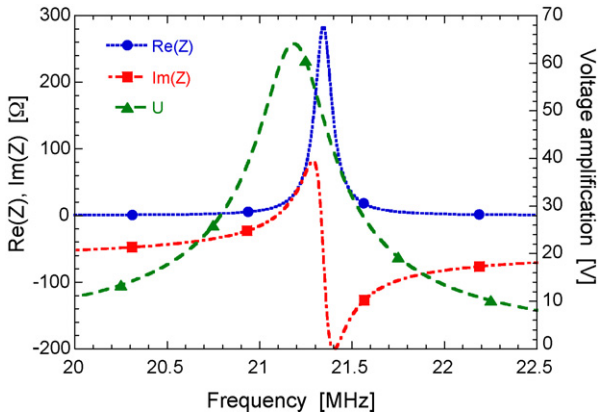

Fig. 4. Simulated curves of complex impedance Z and voltage U for a 1 V input signal. If the values of the discrete elements are properly chosen, both $\mathrm{Re}(Z) = 50\,\Omega$ and maximum voltage amplification occur at the same frequency (here 21.2 MHz).

after the tuning procedure: $\mathrm{Re}(Z) = 50\,\Omega$ and $\mathrm{Im}(Z) = 0\,\Omega$ occur at 21.2441 MHz.

4. Results and discussion

Fig. 7 shows a bright and stable plasma discharge generated in one of the fabricated devices operated in a 50 mbar He atmosphere. The transmitted RF power required to ignite the discharge was 350 mW at a frequency near 20 MHz (the plasma is readily ignited within 1 MHz of the "ideal" frequency). In general, the plasma discharges cover uniformly the entire electrode area as shown in Fig. 7.

We have successfully ignited plasmas with electrode gaps ranging from 10 to 500 μm, in three gases (He, Ar and N_2), and with different electrodes geometries including corrugated edges to enhance the electric field and reduce the voltage (hence power) required for ignition. Due to limits of the anodic bonding equipment, the complete triple-stack devices could be hermetically sealed only either under high vacuum or under a pressure of

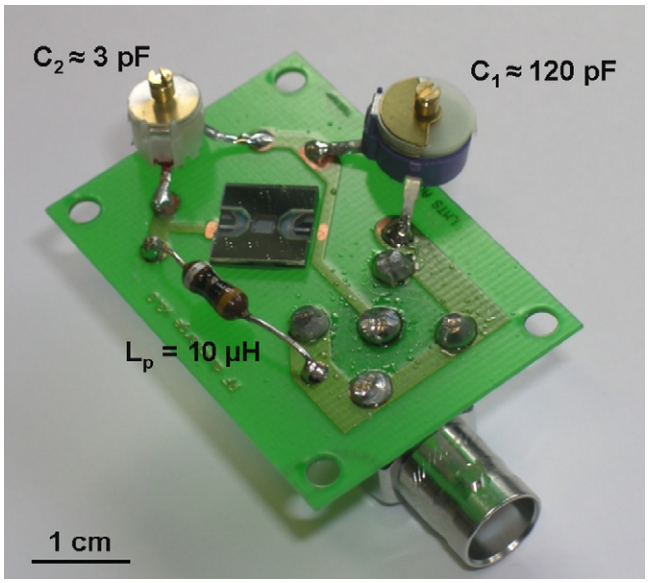

Fig. 5. The completed MEMS chip is mounted on a PCB with the discrete elements (two trimmer capacitors and one fixed-value inductor) to implement the impedance matching circuit.

450 mbar of Nitrogen. For the study of the influence of the gas type and pressure on the plasma, we operated devices in a vacuum chamber without the final cap layer (i.e., devices from step "h" of Fig. 1). Modifications to the setup are underway to allow sealing under arbitrary gas type and pressure.

Optical spectra of the plasma are acquired with a USB4000 fiber-optic spectrometer from Ocean Optics by placing a multimode optical fiber (600 μm core diameter) on top of the device. Fig. 8 shows measured spectra of plasma discharges in He, Ar and N_2. These spectra reveal the expected different peak patterns characteristic of each gas. In addition to showing that the chip-scale plasmas can be used as a light source, spectroscopy of the emitted light as

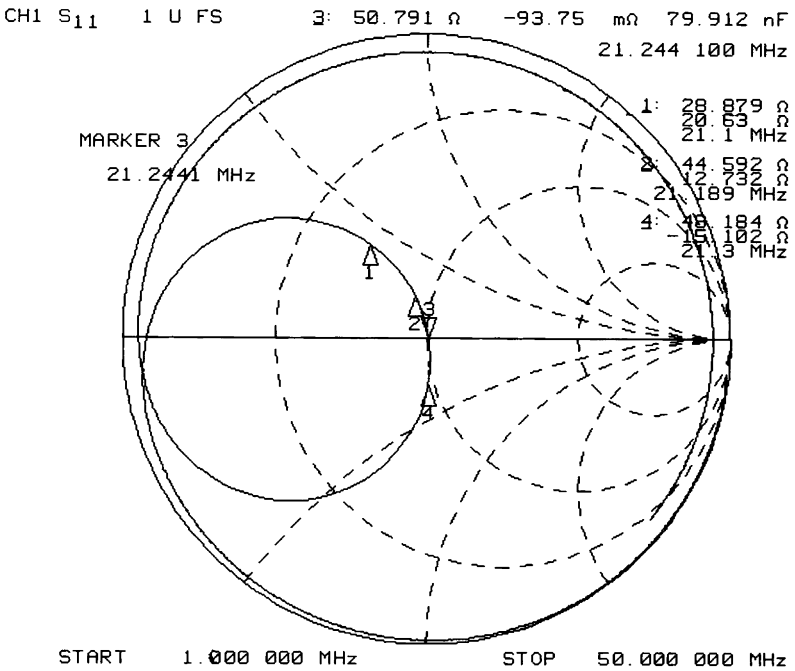

Fig. 6. Smith chart displaying the impedance of the circuit in Fig. 5 measured between 1 and 50 MHz. Accurate 50 Ω matching is achieved at 21.244 MHz.

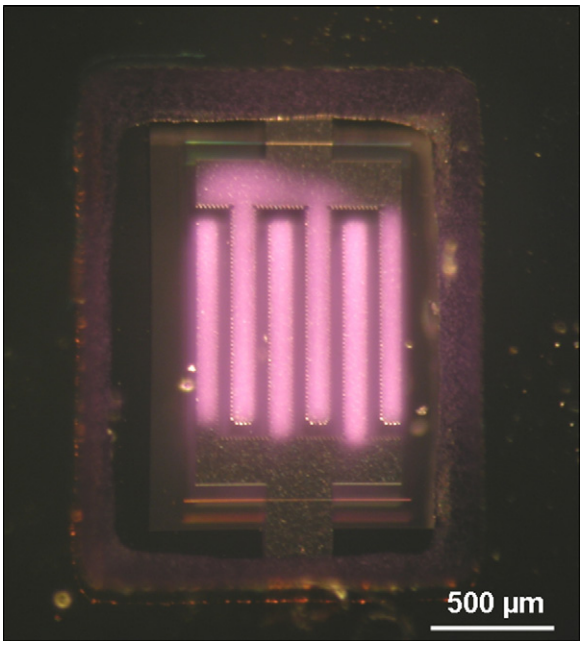

Fig. 7. Optical micrograph showing a stable plasma discharge ignited in He (50 mbar) covering the whole area above the interdigitated electrodes. The transmitted power required for ignition was 350 mW at 20 MHz.

in Fig. 8 could be used to identify and quantify leaks or outgassing in a sealed device.

As is well known from Paschen curve studies, different gases require different minimum DC electric fields to ignite a stable plasma. Helium is one of the easiest gases to ignite a plasma, while Nitrogen requires higher fields. This is indeed what we observe for our 20 MHz RF discharges: plasmas in Helium are readily ignited with RF power larger than 300 mW (lower power levels are possible but for a more limited pressure range), in Ar 600 mW is needed, while in Nitrogen 2 W is required for a given electrode geometry and using a given impedance matching circuit. This data comparing different gases was taken on electrodes with a 20 μm gap. Reference [15] presents a study of the effect of gap size and pressure on breakdown voltage.

Fig. 9 is a plot of measured irradiance and optical power as a function of applied RF power for several optical emission peaks for plasmas in Helium at 450 mbar and for Argon at 300 mbar. Irradiance increases approximately linearly with RF power, except near the ignition threshold. The relative intensity of the peaks depends on the RF power. Since the efficiency (optical power/RF power) of light emission increases quickly near ignition, for efficient operation as a light source the applied RF power should be at least 20% greater than the value required for ignition.

Optical power was also measured as a function of pressure for operation in Helium with an RF power of 1.5 W and was found to be only weakly dependent on pressure: optical power was 20% larger at 300 mbar than at 800 mbar. To make an efficient light source, it is therefore desirable to operate at low pressures, both to maximize the optical output, and because the plasmas can be ignited with lower RF power at low pressures.

Continuous operation for several hours at constant power levels up to 1.5 W has been demonstrated without degradation of the electrodes for He and Ar. One device was operated for 24 h in 250 mbar of Argon at 1.5 W transmitted power. One should note that the devices are intended for operation at powers below 100 mW, so this is an accelerated test. After 24 h of continuous operation at 1.5 W the Al electrode thickness (measured using a white light optical

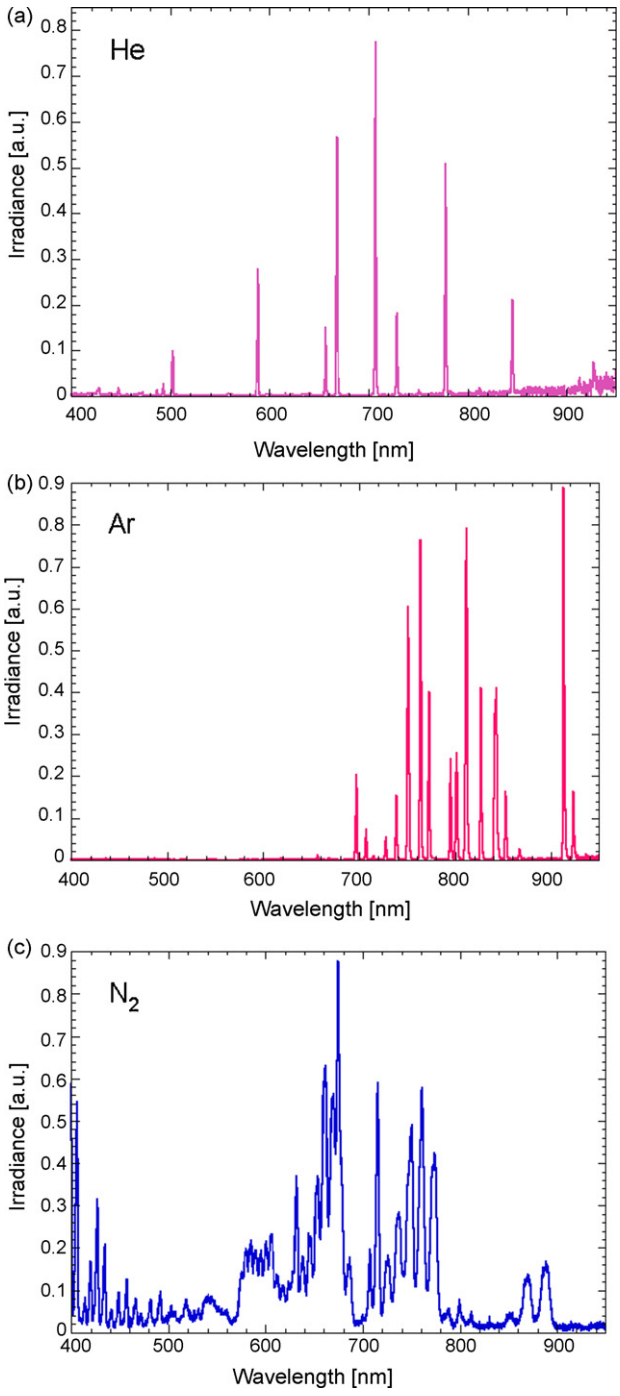

Fig. 8. Optical spectra of plasma discharges on the microfabricated chips ignited: (a) in Helium at 50 mbar with 350 mW RF power, (b) in Argon at 20 mbar with 650 mW, and (c) in Nitrogen at 5 mbar with 4 W.

profilometer) was reduced by 0.3 μm from 6.8 to 6.5 μm, showing that sputtering of the electrodes is occurring. Within our measurement accuracy, the optical power emitted did not change over the duration of the test. Since the plasma is RF rather than DC powered, the electrode lifetime could be enhanced if necessary by adding an extra passivation step to the fabrication process, i.e., by depositing a dielectric film such as SiO_2, Si_3N_4 or Al_2O_3 on top of the Al electrodes. The lifetime of a sealed device might be reduced if sputtered metal or dielectric accumulates on the top (cap) Pyrex chip, decreasing the intensity of light emitted from the chip, even if the

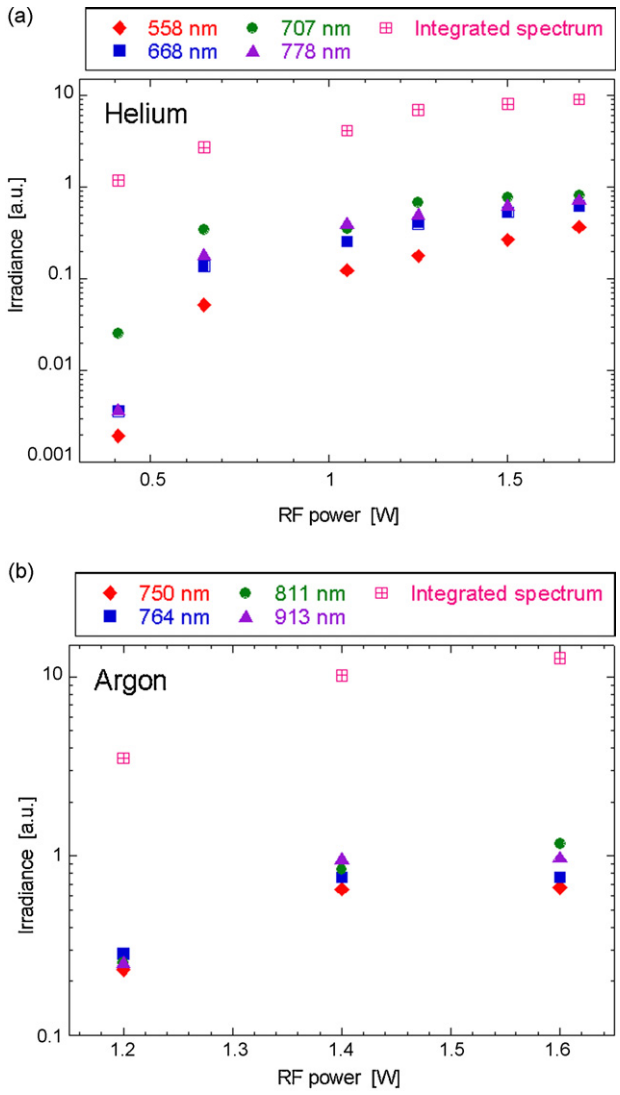

Fig. 9. Measured irradiance vs. transmitted RF power for plasmas in (a) He and (b) in Ar. The irradiance (arbitrary units) for selected peaks are shown, as well as the total power (integrated from 400 to 950 nm).

light intensity from the plasma remains constant. It is thus important to minimize sputtering of the electrodes by operating at lower power or higher frequency.

Heating of the chip and elements in the impedance matching circuit was observed after extended operation at power levels over 1 W, mostly due to the losses in the impedance matching circuit. For a hermetically sealed device, achieving long lifetimes will probably require limiting the power levels in view of the poor thermal conduction of Pyrex.

5. Conclusion

A microfabrication process has been developed to fabricate hermetically sealed cells enclosing passivated or unpassivated Aluminum electrodes in a mm-scale cavity. The process is based on the anodic bonding of three Pyrex wafers enabled by the use of sputter-deposited amorphous silicon. The electrodes are buried within the bottom wafer. Powder blasting is used to create through-holes of arbitrary geometry in the top two chips. When powered through an impedance matching circuit, these devices have been used to generate millimeter-size RF plasma discharges operating continuously in He or Ar at pressures ranging from 10 to 500 mbar at forward RF powers of 300–1500 mW.

Work is ongoing to determine an optimum electrode geometry allowing for the ignition of a stable and long-term operation glow discharge with the lowest RF power level at a given gas pressure. This chip-scale plasma light source will find applications in chip-scale atomic clocks (once filled with Rb or Cs) and allows direct spectroscopy of gases in sealed cavities, for instance for long-term leak testing of wafer-level packaged devices.

Acknowledgements

The authors thank D. Bouvet at LEG1-EPFL for help with the CMP process, J. Gerrits at the CSEM for generous help with all matters RF, P. Rochat of SpectraTime for suggesting the matching network, and C. Schori of the University of Neuchatel for hermetic sealing of the cells. The authors acknowledge financial support from the CIMENT (EPFL – Université de Neuchâtel) program and from the Fondation en faveur d'un Laboratoire de Recherches Horlogères (FLRH).

References

[1] L. Baars-Hibbe, C. Schrader, P. Sichler, T. Cordes, K.-H. Gericke, S. Büttgenbach, S. Draeger, Micro-structured electrode arrays: high-frequency discharges at atmospheric pressure—characterization and new applications, Vacuum 73 (2004) 327–332.
[2] V. Karanassios, Microplasmas for chemical analysis: analytical tool or research toys? Spectrochim. Acta B 59 (2004) 909–928.
[3] J.A. Wright, R.A. Miller, E.G. Nazarov, Atmospheric pressure air microplasma ionization source for chemical analysis applications, in: Tech. Dig. IEEE MEMS'06 Conference, Istanbul, Turkey, January 22–26, 2006, pp. 378–381.
[4] O.P. Naji, A. Manz, A double plasma gas chromatography injector and detector, Lab Chip 4 (2004) 431–437.
[5] U. Engel, A.M. Bilgiç, O. Haase, E. Voges, J.A.C. Broekaert, A microwave-induced plasma based on microstrip technology and its use for the atomic emission spectrometric determination of mercury with the aid of the cold-vapor technique, Anal. Chem. 72 (2000) 193–197.
[6] G. Jenkins, J. Franzke, A. Manz, Direct optical emission spectroscopy of liquid analytes using an electrolyte as a cathode discharge source (ELCAD) integrated on a micro-fluidic chip, Lab Chip 5 (2005) 711–718.
[7] P. Carazzetti, Ph. Renaud, H. Shea, Low-power hermetically sealed on-chip plasma light source micromachined in glass, in: Tech. Digest IEEE 21st International Conference on Micro Electro Mechanical Systems (MEMS 2008), pp. 818–821.
[8] F. Paschen, Über die zum Funkenübergang in Luft, Wasserstoff und Kohlensäure bei verschiedenen Drucken erforderliche Potentialdifferenz, Annalen der Physik 273 (5) (1889) 69–96.
[9] R.S. Dhariwal, J.M. Torres, M.P.Y. Desmulliez, Electric field breakdown at micrometre separations in air and nitrogen at atmospheric pressure, IEE Proc. Sci. Meas. Technol. 147 (5) (2000) 261–265.
[10] J.-M. Torres, R.S. Dhariwal, Electric field breakdown at micrometre separations, Nanotechnology 10 (1999) 102–107.
[11] P.G. Slade, E.D. Taylor, Electrical breakdown in atmospheric air between closely spaced (0.2 μm–40 μm) electrical contacts, IEEE Trans. Comp. Packaging Technol. 25 (3) (2002) 390–396.
[12] A. Wallash, L. Levit, Electrical breakdown and ESD phenomena for devices with nanometer-to-micron gaps, Proc. SPIE 4980 (2003) 87–96.
[13] C.-H. Chen, J.A. Yeh, P.-J. Wang, Electrical breakdown phenomena for devices with micron separations, J. Micromech. Microeng. 16 (2006) 1366–1373.
[14] F.W. Strong, J.L. Skinner, P.M. Dentinger, N.C. Tien, Electrical breakdown across micron scale gaps in MEMS structures, Proc. SPIE 6111 (2006) 611103.
[15] P. Carazzetti, Ph. Renaud, H. Shea, Experimental study of electrical breakdown in MEMS devices with micrometer scale gaps, Proc. SPIE Photonics West (2008) 6884–6892.
[16] J.C.T. Eijkel, H. Stoeri, A. Manz, A molecular emission detector on a chip employing a direct current microplasma, Anal. Chem. 71 (1999) 2600–2606.
[17] C. Schrader, et al., Micro-structured electrode arrays: glow discharge in Ar and N2 at atmospheric pressure using a variable radio frequency generator, Vacuum 80 (2006) 1144–1148.
[18] V.G. Kutchoukov, F. Laugere, W. van der Vlist, L. Pakula, Y. Garini, A. Bossche, Fabrication of nanofluidic devices using glass-to-glass anodic bonding, Sens. Actuators A 114 (2004) 521–527.
[19] A.-G. Pawlowski, E. Belloy, A. Sayah, M.A.M. Gijs, Powder blasting patterning technology for microfabrication of complex suspended structures in glass, Microelectron. Eng. 67–68 (2003) 557–565.
[20] Icoflex Sàrl, PSE-A, CH-1015 Lausanne, Switzerland, http://www.icoflex.com.
[21] PSpice module of Cadence OrCAD, http://www.cadence.com/orcad.